Acta Physica Polonica B Proceedings Supplement **18**, 5-A32 (2025)

FORWARD PHYSICS IN ATLAS*

Maciej Trzebiński
on behalf of the ATLAS Collaboration

Institute of Nuclear Physics Polish Academy of Science
Radzikowskiego 152, 31-342 Kraków, Poland

Received 15 April 2025, accepted 16 April 2025, published online 26 June 2025

Processes with scattered protons present in the final state, hereafter called forward physics, are briefly described. ATLAS sub-detectors, ALFA and AFP, dedicated to measure scattered protons, are shown. A few analyses using data collected by these detectors are presented. Namely, elastic scattering at $\sqrt{s} = 7$, 8, and 13 TeV, exclusive di-pion and di-lepton production, and a search for the axion-like particles.

DOI:10.5506/APhysPolBSupp.18.5-A32

1. Forward Physics at the LHC

The LHC collides protons at an unprecedented centre-of-mass energy of $\sqrt{s} = 13.6$ TeV. Such high energy is possible *i.a.* due to both beams being accelerated and colliding. Unfortunately, this imposes beams entering the detectors from two sides, leaving, contrary to fixed target experiments, significant holes in the pseudo-rapidity (η) acceptance. In the ATLAS [1] case, the "main" detectors cannot detect particles having the pseudo-rapidity $|\eta| > 4.9$. To recover part of the acceptance, dedicated devices called Forward Detectors are installed. In the case of ATLAS, these are Zero Degree Calorimeters (ZDC) [1] and ATLAS Roman Pots (ARP) [2, 3]. The former ones allow for measurement of neutral particles, such as neutrons and photons, produced at $|\eta| > 8.3$. The latter ones, which are the scope of this paper, allow for measuring protons that lost a fraction of their energy, $\xi = 1 - \frac{E_{\mathrm{proton}}}{E_{\mathrm{beam}}}$.

Having intact protons in the final state implies that the interaction must not alter their quantum numbers, such as colour or electric charge. A case of electromagnetic exchange is, in a sense, obvious since a photon is colourless. In the case of the strong force, an object that allows for colourless exchange

* Presented at the 31st Cracow Epiphany Conference on the *Recent LHC Results*, Kraków, Poland, 13–17 January, 2025.

is called a Pomeron. To a first approximation, it can be depicted as two gluons carrying compensating colour–anticolour, resulting in a colour-neutral object. In reality, the Pomeron structure is, analogous to that of the proton, much richer containing a "sea" of quarks, anti-quarks, and gluons. The Pomeron structure is often described in terms of Diffractive Parton Distribution Functions (DPDF) [4, 5].

The possibility to recognize events having a proton on one or both sides enhances the ATLAS physics programme.

1.1. Diffractive processes

For decades, diffraction has been an important part of the studies performed in particle physics experiments [6]. Unfortunately, despite all these efforts, there are still many mysteries in this field. In the LHC era, both theoreticians and experimentalists work on various aspects of diffractive measurements. In the community, it is commonly agreed that input from the LHC data is crucial.

Diffraction can be either of soft or hard nature, the latter one being defined as a kinematic regime where perturbative calculations can be effectively applied. Considering the properties of the final states, this suggests particles with high transverse momenta produced in the collision. Soft diffractive processes, shown in figures 1 and 2, can be divided into classes:

— elastic scattering — a $pp \to pp$ process in which momentum is transferred between interacting protons and no particles other than the two protons are present in the final state,

— single diffractive dissociation, also called single diffraction — a $pp \to pX$ process, in which the X system has quantum numbers corresponding to the proton ones,

— double diffractive dissociation, also called double diffraction — a $pp \to YX$ process, with a rapidity gap[1] between X and Y systems,

— central diffractive production, also called central diffraction or double Pomeron exchange process: $pp \to pZp$[2], where Z denotes a net-colourless system *e.g.* $Z = \pi^+\pi^-$ as shown in figure 2 (rightmost).

In all of these cases, due to the colourless nature of the exchange, an experimental signature is a so-called rapidity gap present between the proton(s) and produced systems. In non-diffractive production, $pp \to X$, rapidity

[1] A space in rapidity devoid of produced particles.

[2] Also $pp \to pZX$ and $pp \to YZX$, where X and Y systems carry the proton quantum numbers.

gaps can also appear. However, since they result only from fluctuations in particle production in the pseudo-rapidity phase space, the probability of having events with large gaps is very small.

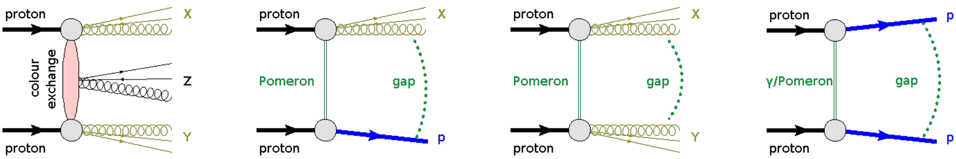

Fig. 1. From left to right: Feynman diagrams for the soft non-diffractive, single diffractive, double diffractive production, and elastic scattering.

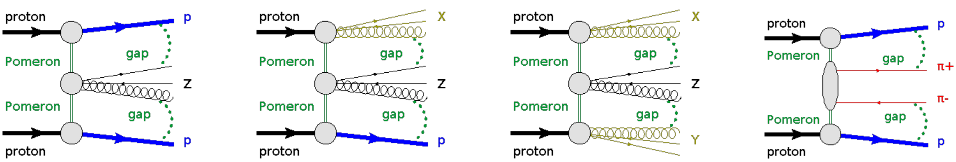

Fig. 2. From left to right: Feynman diagrams for three classes of central diffraction and an exact example of exclusive pion (continuum) production.

There is a variety of hard diffractive processes that can be studied at the LHC. To mention a few examples:

— single diffractive and Double Pomeron Exchange (DPE) di-jet, jet–gap–jet, and photon+jet,

— single and double Pomeron exchange W and $t\bar{t}$,

— exclusive jet production.

To give a better idea about the expected signatures, the examples of corresponding Feynman diagrams are presented in figure 3.

Studies of properties of these events should allow for investigations of many interesting aspects of diffractive physics, with a few examples given below.

— Structure and nature of Pomeron. DPDFs were measured at HERA and then used for LHC energies, meaning that the extrapolation should be verified.

— Factorisation tests (gap survival factor). A check of DPDFs universality, *i.e.*, whether the collinear factorisation [7] holds or not. DPDFs were extracted from the high-precision HERA data, and the factorisation theorem was studied using diffractive di-jet cross sections in Deep

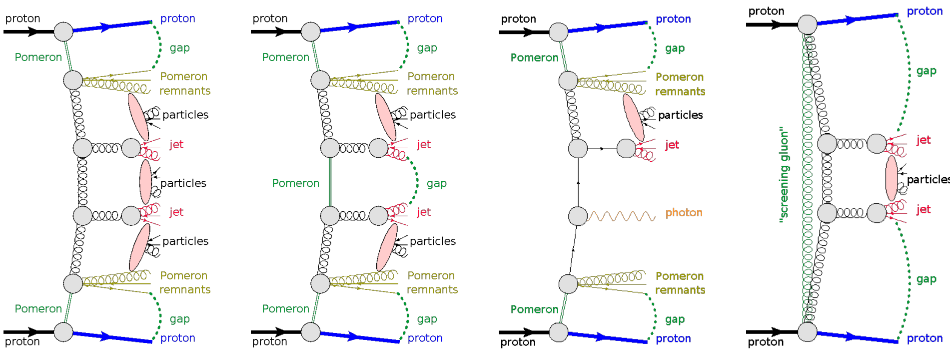

Fig. 3. From left to right: Feynman diagrams for double Pomeron exchange di-jet, jet–gap–jet, photon+jet, and exclusive di-jet production processes.

Inelastic Scattering [8–10]. However, hard scattering factorisation was observed to break down in $p\bar{p}$ collisions at the Tevatron [11], where the cross section for the single diffractive di-jet production was overestimated by an order of magnitude. This breakdown was shown to be explainable by "screening" effects, quantified by the rapidity gap survival probability. Interpretation of the gap survival factor is quite well established, but the existing models have large uncertainties on the values predicted for the LHC [12].

— Colourless exchange within the hard system. Forward physics allows for addressing specific aspects of the QCD dynamics, notably the BFKL and small-x physics. The Balitsky–Fadin–Kurayev–Lipatov (BFKL) Pomeron [13–15] has been originally introduced for the high-energy scattering of partons, but now also includes aspects of integrability and the connection with gravity and string theory. Consequently, there is a strong motivation to establish its existence in the field of strong interactions.

1.2. Photon-induced processes

Another interesting class with scattered proton(s) in the final state are the so-called photon-induced processes. An example is exclusive di-lepton production, shown in figure 4, left. This Standard Model process is important for a wide range of astrophysical phenomena, such as cosmic gamma rays or neutron stars. Measurements at the LHC provide fundamental tests of quantum electrodynamics in controlled, laboratory conditions.

Photon-induced processes may also result in beyond the Standard Model (BSM) signatures. One example are Anomalous Gauge Couplings: $\gamma\gamma \to \gamma\gamma$, $\gamma\gamma \to WW$, $\gamma\gamma \to ZZ$ or $\gamma\gamma \to \gamma Z$. Accordingly to feasibility studies de-

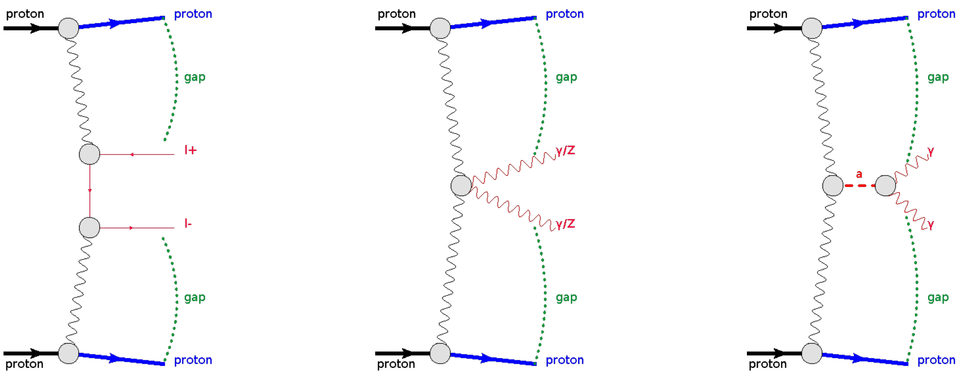

Fig. 4. From left to right: Feynman diagrams for photon-induced processes: exclusive di-leptons, (Quartic) Anomalous Gauge Couplings and axion-like production processes.

scribed in Ref. [16], the possibility of reducing background by using a proton-tagging technique may result in sensitivities better by 2 orders of magnitude w.r.t. "standard" methods. This "background reduction advantage" can be applied to other processes. One example is Axion-like Particle (ALP) production, see figure 4, right, which can appear as a resonance decaying into two photons or as a loop coupled to photons.

2. Forward Proton detectors

The ATLAS Roman Pots consist of two subsystems: Absolute Luminosity For ATLAS (ALFA) [2] and ATLAS Forward Proton (AFP) [3]. These devices were constructed in the so-called Roman Pot technology, which allows for detector movement w.r.t. the LHC beam. In non-stable beam conditions (*e.g.* injection), detectors are far away ($\mathcal{O}(40)$ mm) from the beam. Once the beams are declared stable, the detectors approach them to a certain distance, usually of about 1–4 mm. Accordingly to the LHC safety rules, the Pot insertion depends on the properties of beams (*e.g.* intensity) and settings of LHC magnets (so-called optics).

ALFA was designed to precisely measure properties of the elastic scattering process. Due to the nature of this process, detectors are installed fully symmetrically around the ATLAS Interaction Point (IP). There are two stations on each side of IP, located 237 and 241/245 m from the center of the ATLAS detector[3]. Each station hosts two Roman Pots moving vertically (from the top and bottom) towards the beam. Each Pot contains a set of 2×10 layers of 64 scintillating fibres arranged in a so-called U–V

[3] During LHC Long Shutdown 1, stations were moved from 241 to 245 m.

geometry. The fibre size is 0.5 mm, but due to plane staggering, the overall spatial resolution is about 30 μm. The chosen technology results in almost edgeless detectors, enabling measurements as close to the beam as possible. The fibres were aluminised to reduce light losses and optical cross-talk.

The AFP detectors are horizontally moving stations installed symmetrically with respect to the ATLAS IP at 205 (NEAR) and 217 (FAR) meters. Stations located closer to the IP contain a tracker (3D edgeless silicon pixel detectors), whereas the outer ones are also equipped with Time-of-Flight (ToF) devices. The reconstruction resolution of tracking detectors is about 6 and 30 μm in x and y, respectively [17]. The current version of the Time-of-Flight detector has a resolution of about 25 ps [18]. Unfortunately, during the Run 2 data-taking, their efficiency was low — see Ref. [18].

3. Glimpse on analysis

The ALFA detectors were already installed for the LHC Run 1. Since 2011, they have been taking data in several dedicated campaigns, with the last data-taking done in 2023. A summary of the data-taking campaigns is given in Table 1. An indication of kinematic regions accessible with a given data-set is shown in figure 5 (left).

Table 1. Summary of data-taking campaigns in which ALFA participated.

Year	$\sqrt{s}$ [TeV]	β^* [m]	Comments
2011	7	90	main goal: elastics measurement; parasitic data for diffractive analyses
2012	8	90	goals as above
2012	8	1000	elastics analysis targeting Coulomb-Nuclear Interaction (CNI) region
2013	5.02	0.8	proton–lead collisions
2013	5.02	0.8	proton–proton reference run
2015	13	90	main goal: diffractive measurements
2016	13	2500	main goal: elastics analysis targeting CNI
2018	13	90	elastic measurement at large momentum transfer, t, diffractive analyses
2018	0.9	11	elastic measurement at large-t
2018	0.9	50/100	elastics analysis targeting CNI
2023	13.6	3000/6000	goals as above

3.1. ALFA: elastic scattering

The original goal of ALFA was to provide the absolute scale for the ATLAS luminosity measurements [20]. This would require access to very low values of the four-momentum transfer, t — a region where Coulomb interactions dominate. Such desire resulted in the need for operation using special settings of the LHC magnets — so-called high-β^* optics [19]. In reality, collected data allowed for measuring:

— total (σ_{tot}), elastic (σ_{el}), and inelastic (σ_{inel}) cross sections, $\frac{\mathrm{d}\sigma}{\mathrm{d}t}$, nuclear slope ($B$) at $\sqrt{s} = 7$ and 8 TeV — see Refs. [21, 22],

— like above, plus a real-to-imaginary ratio of the nuclear elastic scattering amplitude, ρ, at $\sqrt{s} = 13$ TeV — see Ref. [23].

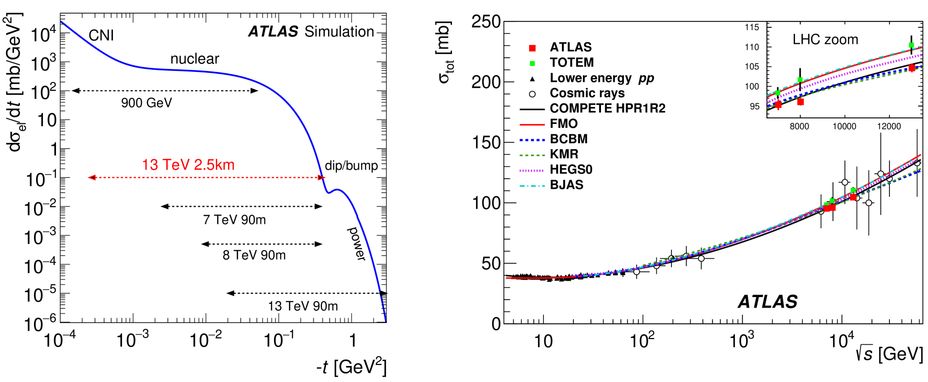

Fig. 5. Left: Predictions of the t-range ALFA coverage in various data-taking campaigns. Right: Energy evolution of the total cross section compared to different model predictions; ATLAS (ALFA) data are marked in red. From Ref. [23].

As one can judge from figure 5, right, the ATLAS results were obtained with unprecedented precision. Interestingly, all ATLAS results systematically differ from the corresponding ones published by the TOTEM Collaboration [24]. An interesting attempt to explain these discrepancies was recently published in Ref. [25].

3.2. ALFA: exclusive pion production

The original ALFA physics programme was extended to measure diffractive physics. One of the motivations, triggered by the feasibility studies from Ref. [26], was the measurement of the exclusive pion production $pp \to p\pi^+\pi^-p$, see figure 2, rightmost. Using 80 $\mu\mathrm{b}^{-1}$ of $\sqrt{s} = 7$ TeV pp data, the fiducial cross section was measured to be:

— $4.8 \pm 1.0(\text{stat.})^{+0.3}_{-0.2}(\text{syst.}) \pm 0.1(\text{lumi.}) \pm 0.1(\text{model})$ μb for elastic and

— $9 \pm 6(\text{stat.})^{+1}_{-1}(\text{syst.}) \pm 1(\text{lumi.}) \pm 1(\text{model})$ μb for anti-elastic configuration — see Ref. [27] for the analysis details.

Another example of diffractive analysis done with ALFA is the measurement of single diffraction at $\sqrt{s} = 8$ TeV [28]. Within the fiducial range of $-4.0 < \log_{10} \xi < -1.6$ and $0.016 < |t| < 0.43$ GeV^2, the cross section was measured to be $\sigma_{\text{SD}} = 1.59 \pm 0.13$ mb.

3.3. AFP: exclusive di-lepton production

While ALFA took data only during dedicated LHC fills, AFP was designed to participate in all data-taking periods. The possibility of collecting data at high pile-up resulted in access to low cross-section processes. One such example is the exclusive di-lepton production, see figure 4, left. With 14.6 fb^{-1} of $\sqrt{s} = 13$ TeV pp data, AFP identified 57 (123) candidates in the $ee(\mu\mu)$ final state, which translates to the fiducial cross section of

— $\sigma_{ee} = 11.0 \pm 2.6(\text{stat.}) \pm 1.2(\text{syst.}) \pm 0.3(\text{lumi.})$ fb and

— $\sigma_{\mu\mu} = 7.2 \pm 1.6(\text{stat.}) \pm 0.9(\text{syst.}) \pm 0.2(\text{lumi.})$ fb.

These candidates are shown in figure 6, left. More details about this analysis can be found in Ref. [29].

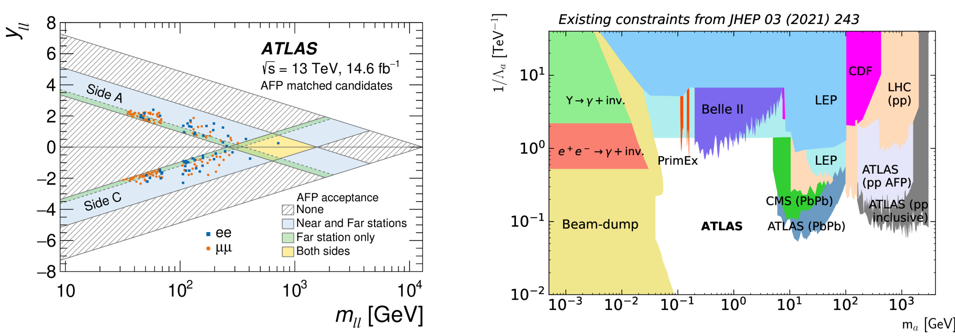

Fig. 6. Left: Exclusive di-electron (blue) and di-muon (orange) candidates registered by AFP in the 2017 data-set. From Ref. [29]. Right: AFP contribution to the global search for the BSM particles. From Ref. [30].

3.4. AFP: search for axion-like particles

An example of BSM analysis is a search for the ALPs. As shown in figure 4, right, such particles can be produced in $\gamma\gamma \to a \to \gamma\gamma$ process, leaving both protons intact. The search was done using the same dataset as in the case of the exclusive di-leptons. After a careful event selection, 441 signal candidates were identified [30]. A search was made for a narrow resonance in the di-photon mass distribution, corresponding to an ALP with a mass in the range of 150–1600 GeV. No excess above the background was observed. Assuming the 100% decay branching ratio into a photon pair, the upper limit on the coupling constant was set to be in the range of 0.04–0.09 TeV at 95% confidence level. A contribution of this measurement to the global search for the BSM particles is shown in figure 6, right.

4. Summary and outlook

ALFA took several interesting data-sets with special high-β^* optics, which allow access to the small-t region. So far, the focus has been on the elastic analysis. As described in this paper, a few results were already published, while other datasets (especially from 2018 and 2023) are being analysed. In addition, two diffractive results were published.

AFP continues taking data at the low-β^* conditions. Two analyses based on the 2017 high-μ dataset were published and briefly described in this paper. More studies, based on both low-μ (soft and hard diffraction) and high-μ datasets (photon-induced processes, BSM searches), are on the way.

The work of M.T. was partially supported by the National Science Centre (NCN), Poland (project No. UMO-2019/34/E/ST2/00393).

REFERENCES

[1] ATLAS Collaboration (G. Aad *et al.*), *J. Instrum.* **3**, S08003 (2008).
[2] S. Abdel Khalek *et al.*, *J. Instrum.* **11**, P11013 (2016).
[3] ATLAS Collaboration, «Technical Design Report for the ATLAS Forward Proton Detector», CERN-LHCC-2015-009, ATLAS-TDR-024.
[4] H1 Collaboration (A. Aktas *et al.*), *Eur. Phys. J. C* **48**, 749 (2006).
[5] ZEUS Collaboration (S. Chekanov *et al.*), *Nucl. Phys. B* **831**, 1 (2010).
[6] E. Predazzi, `arXiv:hep-ph/9809454`.
[7] J.C. Collins, *Phys. Rev. D* **57**, 3051 (1998); *Erratum ibid.* **61**, 019902 (1999).
[8] H1 Collaboration (A. Aktas *et al.*), *J. High Energy Phys.* **2007**, 042 (2007).
[9] H1 Collaboration (F.D. Aaron *et al.*), *Eur. Phys. J. C* **70**, 15 (2010).
[10] ZEUS Collaboration (S. Chekanov *et al.*), *Eur. Phys. J. C* **52**, 813 (2007).
[11] CDF Collaboration (T. Aaltonen *et al.*), *Phys. Rev. D* **86**, 032009 (2012).

[12] A.B. Kaidalov, V.A. Khoze, A.D. Martin, M.G. Ryskin, *Eur. Phys. J. C* **21**, 521 (2001).

[13] L.N. Lipatov, *Sov. J. Nucl. Phys.* **23**, 338 (1976).

[14] E.A. Kuraev, L.N. Lipatov, V.S. Fadin, *Sov. Phys. JETP* **45**, 199 (1977).

[15] I.I. Balitsky, L.N. Lipatov, *Sov. J. Nucl. Phys.* **28**, 822 (1978).

[16] Ch. Royon, *SciPost Phys. Proc.* **15**, 029 (2024).

[17] J. Lange *et al.*, *J. Instrum.* **11**, P09005 (2016).

[18] ATLAS Collaboration, «Performance of the ATLAS Forward Proton Time-of-Flight Detector in 2017», ATL-FWD-PUB-2021-002.

[19] M. Trzebiński, *SPIE* **9290**, 929026 (2014).

[20] ATLAS Luminosity and Forward Physics Community, «Technical Design Report», CERN-LHCC-2008-004.

[21] ATLAS Collaboration, *Nucl. Phys. B* **889**, 486 (2014).

[22] ATLAS Collaboration, *Phys. Lett. B* **761**, 158 (2016).

[23] ATLAS Collaboration (G. Aad *et al.*), *Eur. Phys. J. C* **83**, 441 (2023).

[24] TOTEM Collaboration, «Technical Design Report», CERN-LHCC-2004-002.

[25] P. Grafström, R. Staszewski, `arXiv:2502.13618 [hep-ph]`.

[26] R. Staszewski *et al.*, *Acta Phys. Pol. B* **42**, 1861 (2011).

[27] ATLAS Collaboration (G. Aad *et al.*), *Eur. Phys. J. C* **83**, 627 (2023).

[28] ATLAS Collaboration (G. Aad *et al.*), *J. High Energy Phys.* **2020**, 42 (2020).

[29] ATLAS Collaboration (G. Aad *et al.*), *Phys. Rev. Lett.* **125**, 261801 (2020).

[30] ATLAS Collaboration (G. Aad *et al.*), *J. High Energy Phys.* **2023**, 234 (2023).